JACS
JOURNAL OF THE AMERICAN CHEMICAL SOCIETY
pubs.acs.org/JACS
Article

Tailoring Fluorescence–Phosphorescence Emission with a Single Nanocavity

Wei Peng, Yao-Hui Wang, Jiaxing He, Jing-Liang Yang, Jingyu Wang, Petar M. Radjenovic, Jia-Sheng Lin, Zhilin Yang, Ming-De Li, Fan-Li Zhang, Yue-Jiao Zhang, Jun Yi,* and Jian-Feng Li*

Cite This: J. Am. Chem. Soc. 2023, 145, 20381–20388

ABSTRACT: Realizing the dual emission of fluorescence–phosphorescence in a single system is an extremely important topic in the fields of biological imaging, sensing, and information encryption. However, the phosphorescence process is usually in an inherently "dark state" at room temperature due to the involvement of spin-forbidden transition and the rapid non-radiative decay rate of the triplet state. In this work, we achieved luminescent harvesting of the dark phosphorescence processes by coupling singlet-triplet molecular emitters with a rationally designed plasmonic cavity. The achieved Purcell enhancement effect of over 1000-fold allows for overcoming the triplet forbidden transitions, enabling radiation enhancement with selectable emission wavelengths. Spectral results and theoretical simulations indicate that the fluorescence–phosphorescence peak position can be intelligently tailored in a broad range of wavelengths, from visible to near-infrared. Our study sheds new light on plasmonic tailoring of molecular emission behavior, which is crucial for advancing research on plasmon-tailored fluorescence–phosphorescence spectroscopy in optoelectronics and biomedicine.

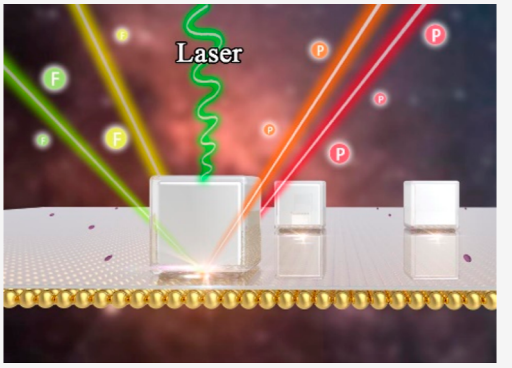

INTRODUCTION

Fluorescence–phosphorescence dual emission in a single system exhibits rich excited-state features and considerable energy differences,[1] which can be used in various applications, such as biological analysis,[2−4] sensing research,[5−7] as well as graphic image and display.[8,9] Continuously regulating emission peak positions, capable of satisfying on-demand remote access under imposed external conditions, is significant for encoding, manipulating, and controlling colors.[10,11] Therefore, precisely tailoring fluorescence–phosphorescence emission with controlled emission spectral peak positions may lead to lots of revolutionary applications for the development of a wide range of research fields.[12,13]

However, unlike singlet state fluorescence, triplet state phosphorescence is typically not observed at room temperature and is mostly only emitted under harsh conditions, such as low temperatures or hypoxia, due to its slow radiation rate and oxygen quenching of excited states.[14,15] Promoting intersystem crossing or effectively suppressing the quenching of phosphorescence are key factors for realizing phosphorescence emission. In general, fabricating a rigid environment and tethering molecules in a solid matrix to suppress the non-radiative decay can lead to efficient phosphorescence emission with a high quantum yield. However, this method suffers from limitations in terms of reproducibility and processability, which restrict its practical application in certain contexts.[15,16] Additionally, phosphorescence properties can be also regulated through the spin–orbit coupling effect of heavy metals or tuning the triplet state energy splitting with delicate molecule design. However, current methods have limitations in the available molecule structures and make it difficult to flexibly and widely tailor the emission peak position.[17]

Noble metal nanostructures exhibiting surface plasmon resonance (SPR) can localize light fields and energy at a subwavelength scale, thus serving as an excellent candidate to modify the emission or scattering behavior of emitters at the single-molecule level.[18−20] It greatly facilitates the development of a series of plasmonic applications, such as plasmon-enhanced fluorescence (PEF),[21−23] surface-enhanced Raman scattering (SERS),[24−26] and plasmon-enhanced phosphorescence (PEP).[27] Both PEF and SERS have achieved major breakthroughs, with intensity enhancement over 4 orders of magnitude, and have become spectroscopic techniques with extraordinary sensitivity and powerful characterization capabilities.[28−30] However, theorists have predicted that metal-enhanced phosphorescence processes are feasible; that is, triplet transitions occur on very short timescales—comparable

Received: May 26, 2023
Published: September 5, 2023

https://doi.org/10.1021/jacs.3c05496
J. Am. Chem. Soc. 2023, 145, 20381−20388

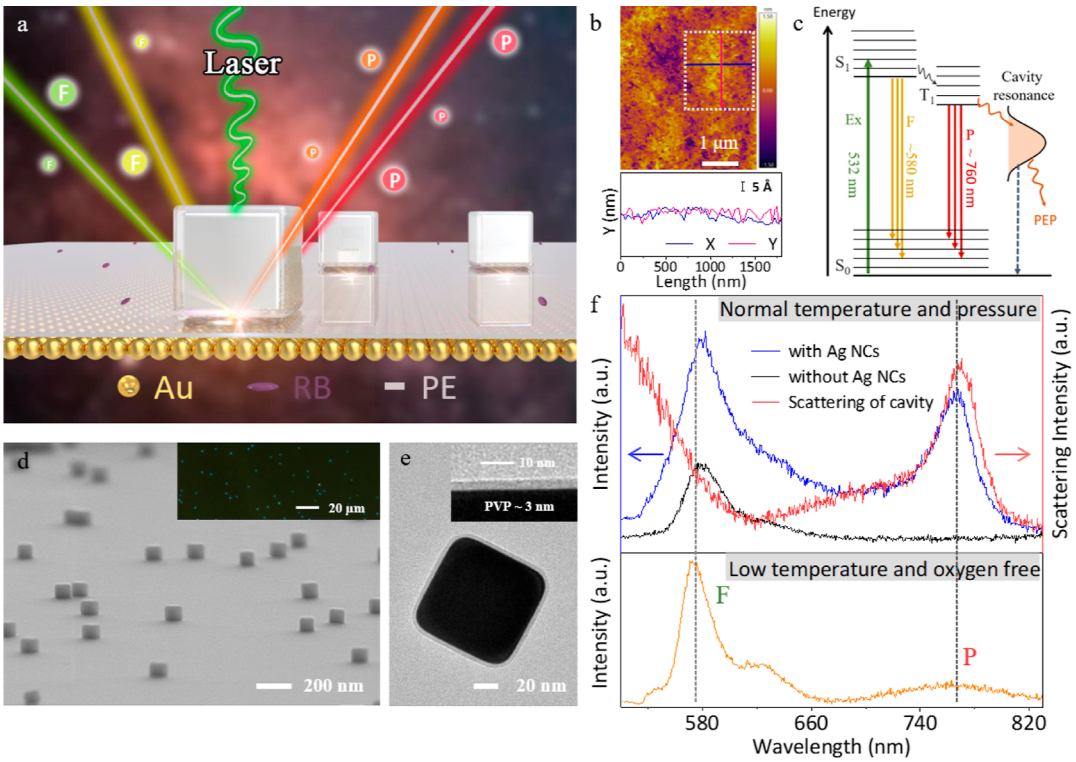

Figure 1. (a) 3D schematic diagram of the model system. (b) AFM image of the ultra-flat Au film. (c) Energy-level diagram of RB and the plasmonic resonance. (d) SEM cross-sectional image of a diluted (10-fold) Ag NC sample. The inset is the dark-field microscopic scattering image of a diluted (1000-fold) Ag NC sample. (e) Transmission electron microscopy images of an Ag NC. Inset is a further magnified view of the protective shell. (f) The bottom panel is the emission spectrum of the RB probe molecules at −190 °C in hypoxic conditions, and the top panel is the emission spectra of the Au film surface with RB probe molecules at room temperature (without Ag NCs, black curve; and with Ag NCs, blue curve) and the corresponding dark-field scattering spectrum (red curve).

to conventional fast transitions—through plasmon coupling.[31,32] However, to date, experiments have shown that PEP exhibits only negligible quantum efficiency (QE) of radiation and modest enhancement factors (~10) at low temperatures because the triplet radiative transition is considerably slower than the non-radiative recombination process.[33−35] Here, we propose a strategy called localized surface plasmon-tailored spectroscopy that allows for tunable peak positions and activation of the phosphorescence emission process at room temperature. Through experimental and theoretical verification, we achieved ultrafast emission of phosphorescence, with spontaneous-emission rate enhancement exceeding 1000 while maintaining a high quantum yield. This has allowed us to overcome the limitations of rapid non-radiative transitions, enabling plasmonic structures to manipulate fluorescence−phosphorescence radiative behavior.

RESULTS AND DISCUSSION

Plasmon-Tailored Fluorescence−Phosphorescence Spectroscopy Model Construction. The plasmonic nanocavity substrate is depicted in 3D in Figure 1a. It consists, from bottom to top, of an ultra-flat Au film, a spacer layer consisting of polyelectrolytes (PEs) modified with fluorophores, and Ag nanocubes (NCs), respectively. Characterized by atomic force microscopy (AFM), the root-mean-square roughness of the Au film is ~3.55 Å (Figure 1b). Ultra-pure Ag NCs were independently dispersed on the PE layer-coated Au film substrate (Figure 1d). The Ag NCs are coated with a protective shell of approximately 3 nm poly(vinylpyrrolidone) (PVP) (Figure 1e). The ultra-flatness of the Au film and the uniformity of the plasmonic particles are critical because the optical properties of this plasmonic cavity are highly dependent on nanometer- or even angstrom-scale variations of the substrate, particle size, and gap spacing.[36,37] The PEs layer, composed of poly(allylamine hydrochloride) (PAH) and polystyrene sulfonate, was assembled layer by layer (Figure S1), acting as an accurate dielectric spacer which separates the Ag NCs from the Au film while situating the probe molecules within the SPR hotspot. The classic photosensitizer, rose bengal (RB), was chosen as the research molecule because it contains both singlet state fluorescence and triplet state phosphorescence (Figures 1c and S2).[38] RB was deposited on the top PE layer by an amidation reaction with PAH (see Methods).

To establish a clear and direct connection between the plasmonic cavity and molecular emission, the concentration of top Ag NCs was optimized to a sufficiently low to realize single-particle spectroscopy (Figure S3), and a home-built confocal microscope was used to obtain the scattering and emission spectrum of every individual cavity. The cavity resonance was determined by dark-field scattering spectroscopy measured from an individual cavity. The typical image and scattering spectrum from a single cavity (3 layers of PE and 80 nm Ag NC) are shown in the inset of Figure 1d,f (red curve). The room-temperature emission from the same cavity was collected with 532 nm laser excitation. For comparison, the emission spectrum from RB molecules on Au substrates with 3 PE layers but without the top Ag NCs is shown as a reference (Figure 1f, black curve). Distinct emission behaviors were observed in those two cases. For molecules coupled without a

https://doi.org/10.1021/jacs.3c05496
J. Am. Chem. Soc. 2023, 145, 20381−20388

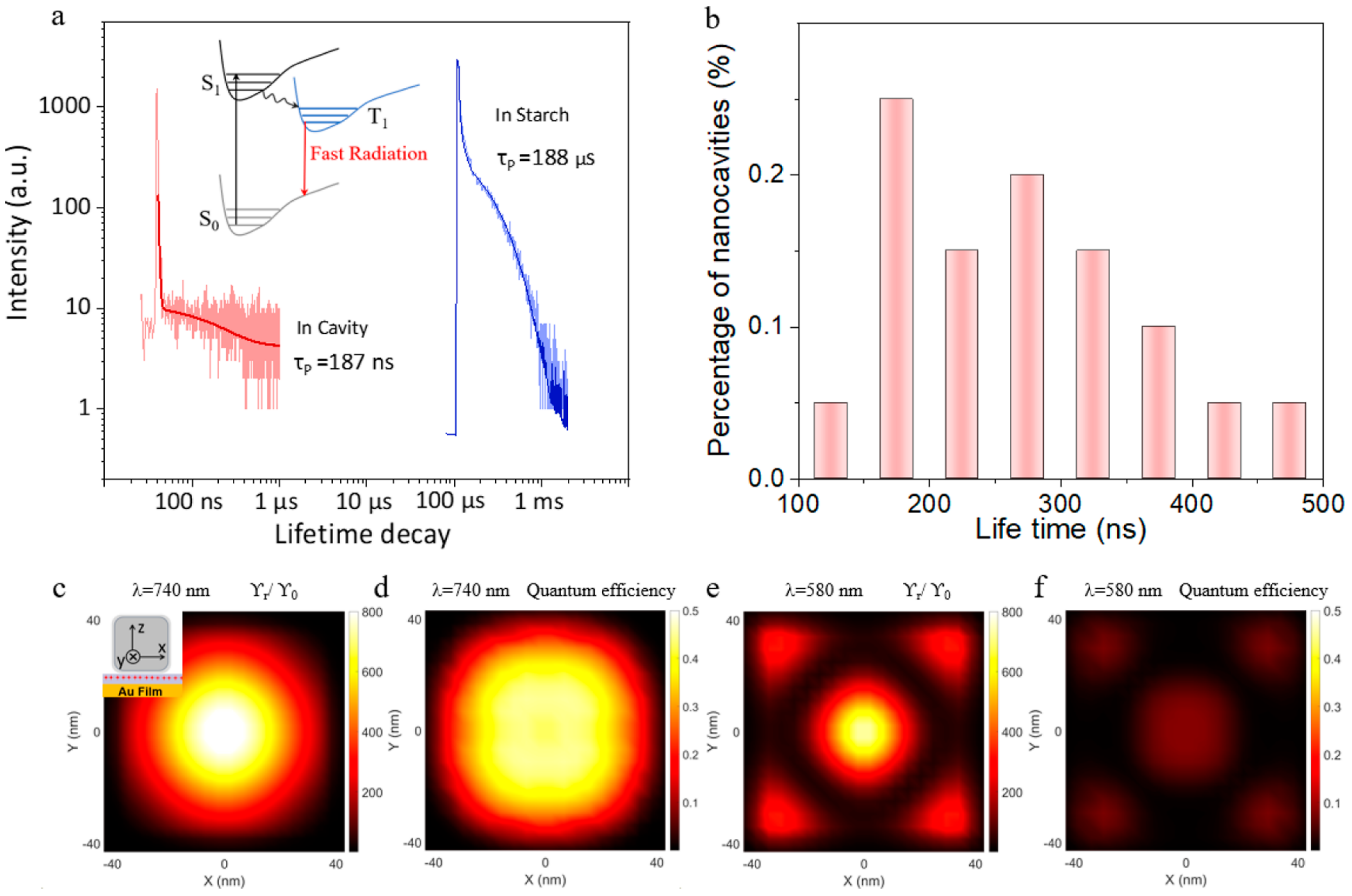

Figure 2. (a) Transient dynamics of RB in starch (blue curve) and in optical cavities (red curve). (b) Histogram of phosphorescence lifetimes of molecules in 20 arbitrarily selected cavities. Simulation of the radiative-rate enhancement (Υ_r/Υ_0) (c) and QE (d) of RB at 740 nm (center of phosphorescence emission) in nanocavity. Simulation of the radiative-rate enhancement (Υ_r/Υ_0) (e) and QE (f) of RB at 580 nm (center of fluorescence emission) in nanocavity.

plasmonic cavity, only the fluorescent peak centering at 580 and 620 nm from singlet state emissions was observed. The emission from triplet states was strongly suppressed due to the optical selection rule as well as oxygen quenching, and it was only observed at cryogenic and anoxic conditions (Figure 1f, orange curve).

Identify the Origin of the Additional Emissions. When the molecules are coupled with the plasmonic cavity, the intensity of the fluorescent peak is slightly enhanced, as expected. However, an additional emission peak centered around 765 nm emerges, which is resonant with the plasmonic cavity and the phosphorescence emissions. To investigate the origin of this additional emission peak, the photoluminescence (PL) of the metal cavity itself was studied. We performed measurements on nanocavities of different sizes (without embedded RB, Figure S4), and no observable features were detected due to the low excitation power and low QE of metal PL. Therefore, we speculate that the emerged emission originates from the RB molecules in the plasmonic cavity. In addition, phosphorescence is highly sensitive to the concentration of oxygen and is commonly used as a distinguishing feature from fluorescence. We performed in situ PL measurements by varying the oxygen concentration and observed a decrease in the intensity of the newly emerged emission peak with increasing oxygen concentration (Figure S5). These results suggest that the dark phosphorescence emission process may be activated by plasmonic cavity coupling.

A straightforward method to distinguish between phosphorescence and fluorescence emission is by observing their distinct emission dynamics. Immobilizing molecules in a solid matrix is a commonly used approach to obtaining room-temperature phosphorescence. Previous studies have reported that the fluorescence lifetime (τ_F) and phosphorescence lifetime (τ_P) of RB in polysaccharide films are typically in the sub-ns and sub-ms ranges, respectively.[39] In our study, we immobilized RB in a starch film and obtained both fluorescence lifetime (τ_F) and phosphorescence lifetime (τ_P). The τ_F and τ_P were found to be 1.5 ns (Table S1 and Figure S6) and 190 μs (blue curve in Figure 2a and Table S2), respectively. More importantly, the τ_P of RB in the cavity (at 740 nm) was also carefully measured. Interestingly, the triplet state of RB in the optical cavity exhibited a dramatically shortened luminescence decay time, with an ultrafast τ_P of 187 ns (red curve in Figure 2a). We recorded the τ_P for 20 arbitrarily selected optical cavities (Figure S8 and Table S3), and as shown in Figure 2b, their lifetimes were all below 500 ns, with 30% of the nanocavities showing sub-200 ns phosphorescence decay times. Furthermore, we examined the PL intensity and lifetime of particles under pulsed laser excitation (Figure S7 and Table S4), with the PL intensity from particles being markedly lower than the emission from molecules within the cavity. Based on these findings, we conclude that the phosphorescence of RB is effectively "activated" within the cavity, exhibiting a significantly faster rate of spontaneous emission. This enhancement

https://doi.org/10.1021/jacs.3c05496
J. Am. Chem. Soc. 2023, 145, 20381−20388

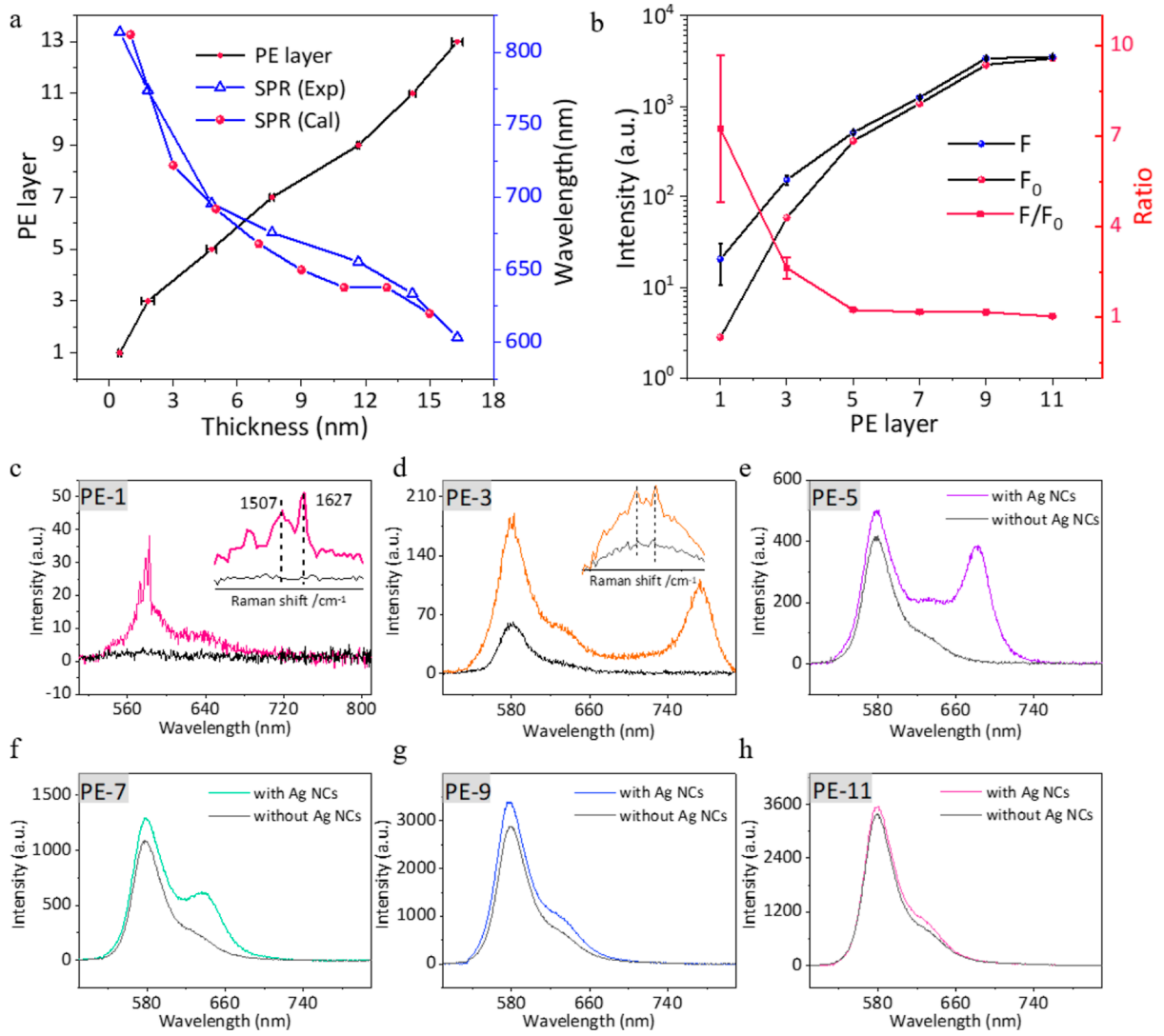

Figure 3. (a) Thickness corresponding to different PE layers (black curve). Corresponding experimentally tested (blue triangle) and theoretically calculated (red circle) SPR peak positions for different-sized cavities. (b) Statistical fluorescence intensities (at 579 nm) in different-sized cavity (F, blue sphere) and control groups (F_0, red sphere). Statistical ratio for F/F_0 (red curve). Error bars in a and b represent s.d. for each data point ($n = 3$ independent experiments) and points are average values. (c–h) PL spectra of molecules in the optical cavity (colored curve) and control group (black curve) under different PE layers. Insets in (c,d) are the locally magnified Raman spectra.

in spontaneous emission rate can be attributed to the Purcell effect.[29] Therefore, in comparison to RB phosphorescence in the starch matrix, the spontaneous-emission rate ($1/\tau_P$) of RB in the cavity increases by more than 1000-fold. The spontaneous emission rate encompasses both radiative and non-radiative transitions. Combining this with the observation that phosphorescence was activated in the steady-state emission spectra, we can conclude that the enhancement of the phosphorescence radiative rate in the cavity far exceeds the non-radiative decay.

Cavity-Modulated Fluorescence–Phosphorescence Emission Dynamics. To clarify the mechanism of the observed molecular fluorescence–phosphorescence emission dynamics, we utilized the finite element method to investigate the differences between plasmonic cavity-modulated fluorescence and phosphorescence emission of RB (see Methods). Figure 2c–f presents maps of the emission properties of RB with 3 layers of PE (PE-3) and an edge length of Ag NCs-80 nm. The reference coordinate system used in the simulation is illustrated in the inset of Figure 2c. The maximal radiative decay rates of the molecule at 740 nm (the center of phosphorescence emission) are almost uniformly enhanced by 800 times due to the increased photonic local density of states (LDOS) (Figure 2c) when coupled with the cavity. It leads to a fast-radiative decay of the phosphorescence emission, also inferred by the significantly reduced lifetime as shown in Figure 2a. More importantly, since the plasmonic cavity mode at 740 nm is dominated by a dipolar mode with large emission efficiency, as a result, the radiative efficiency of the coupled phosphorescence emission is not disturbed by the non-radiative damping. It is quantified by the quantum yield as shown in Figure 2d, which remains high (0.45) and spatially uniform within the cavity. While for the fluorescence emission at 580 nm, the radiative emission rate was also enhanced by approximately 800 times (Figure 2e). However, for the coupling of higher-order cavity modes (at 580 nm), as shown in Figure S11, the radiation efficiency is very weak due to the cancellation of dipole moments caused by the higher-order mode. As a result, the quantum yield of the fluorescence emission is limited to 0.08 (Figure 2f). The results

https://doi.org/10.1021/jacs.3c05496
J. Am. Chem. Soc. 2023, 145, 20381–20388

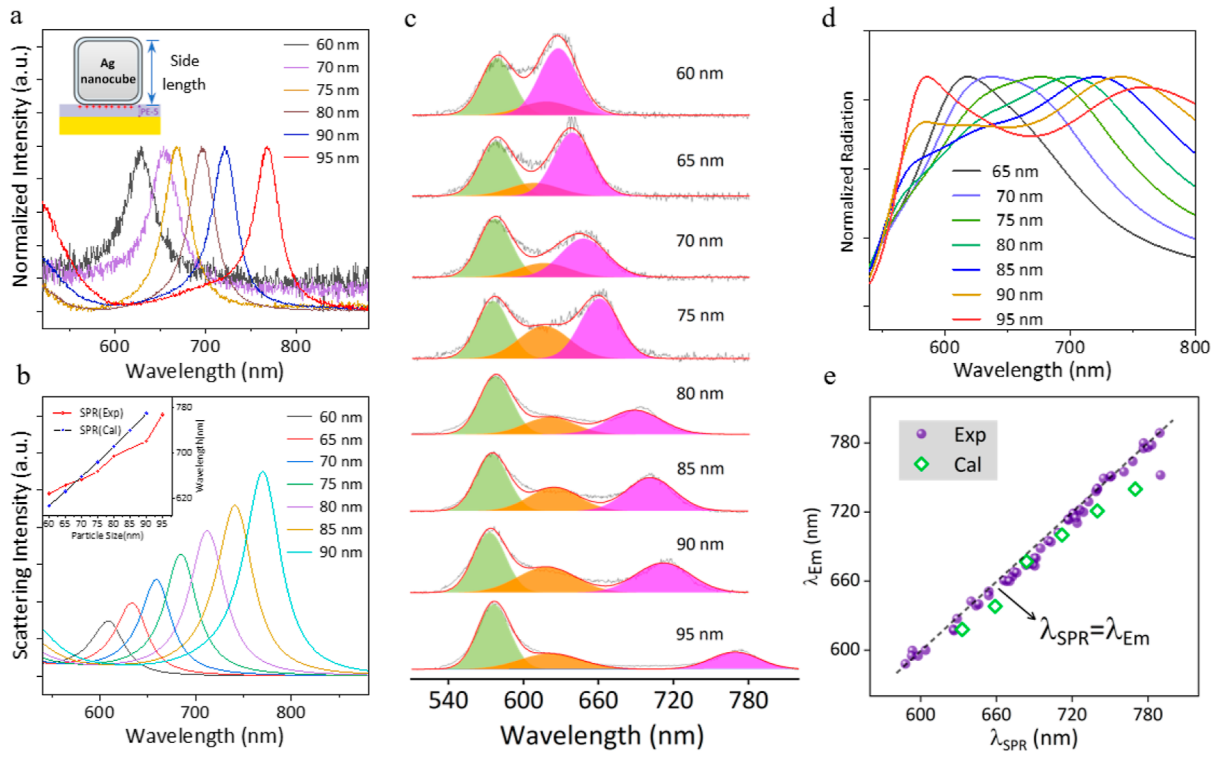

Figure 4. Experimental (a) and calculated (b) SPR spectra as a function of the Ag NC edge length with a fixed cavity size (PE-5). Inset in (b) is the statistical analysis of the experimental and calculated SPR peak positions for Ag NCs with different edge lengths. Normalized experimentally measured PL spectra (c) and calculated radiative behavior (d) of the molecule as a function of the edge length of the Ag NCs with a fixed cavity size (PE-5). (e) Statistical analysis including experimentally measured (purple spheres) and theoretically calculated (green squares) plasmon-induced emission peaks (λ_{Em}) as a function of the corresponding SPR peaks (λ_{SPR}).

indicate that it is possible to control the ratio between fluorescence and phosphorescence emission by modulating the coupling between the cavity mode and molecular emitter.

Since the resonance as well as the LDOS are determined by the size of the plasmonic nanocavity, adjusting the number of PE spacer layers can precisely change the size of the nanocavity. As shown in Figure 3a, the thickness of the spacer can be increased linearly at the nanoscale by increasing the number of PE layers. The uniformity of spacer layer thickness on the same substrate was further verified (Figure S9 and Table S5). With the increase in the number of PE layers, the color of bright spots in the dark-field scattering image changes from green to red (Figure S10). At the same time, the dipole resonances of the SPR spectra exhibit a progressive blue shift from 813 to 603 nm (Figures 3a and S11a). In addition, we calculated the SPR spectra of plasmonic cavities with different sizes (Figure S11b), and the results showed that the peak positions of the theoretically simulated SPR spectra were consistent with the experimental result (Figure 3a, blue line).

The photothermal effect (Figure S12) and hot carrier effect (Figure S13) induced by the excitation light were carefully verified. The results showed that the impact on plasmonic nanostructures and molecules was almost negligible at the power used for the excitation measurements. To investigate the changes in the radiative properties of molecules, we performed the PL measurements on molecules within individual nanocavities of different sizes and compared them with reference optical measurements of control experiments (Figure 3c–h). For the control group (without loaded Ag NCs, black curve), with the increase of the number of PE layers, the fluorescence intensity (F_0, at 579 nm) increases gradually (Figure 3b). When a molecule is in close proximity to the bottom metallic mirror, the energy of the excited molecule is transferred to the metal substrate, resulting in fluorescence quenching. In extreme cases, the fluorescence is completely quenched, such as in the 1 PE layer (PE-1) condition (Figure 3c, black curve).

Compared with the PL spectra of the reference sample, the Raman (1507 and 1627 cm^{-1}) and fluorescence intensity (F, at 579 nm) of the molecules in the cavity both increased (Figure 3c–h, colored curve). The increase in the Raman signal is attributed to the enhancement of the electromagnetic field after loading the plasmonic particles.[40] The enhancement in fluorescence is due to the partial overlap between fluorescence emission and plasmon resonance. The fluorescence enhancement ratio (F/F_0) decreased gradually with the increase of the PE layer (Figure 3b, red curve). A more intuitive contrast is that the emission peak position/spectral shape changes significantly with the number of spacer layers. The singlet-triplet state of the molecule is forced to preferentially emit at the resonant frequency of the optical cavity, thereby changing or even reversing the relative intensities of the vibrational subbands. Although the number of molecules inside the hotspot is much smaller than that outside the hotspot, the molecules at the hotspot experience the strongest radiative enhancement and thus dominate the ensemble emission spectrum[41] (Figures S14 and S15). Nanocavity-coupled photonic environments can effectively tailor the emission peak position of the PL, that is, through the SPR spectrum overlapping with different positions of the molecular emission spectrum. When the optical cavity with larger sizes (Figure 3f–h), the molecule in the cavity experiences a weaker

https://doi.org/10.1021/jacs.3c05496
J. Am. Chem. Soc. 2023, 145, 20381–20388

electromagnetic field, resulting in poor "shaping" of the spectrum.

Tailor the Fluorescence−Phosphorescence Emission. To tailor the fluorescence−phosphorescence emission of RB over a broad wavelength range, we covered the Au film with 5 layers of PE, followed by assembling a series of Ag NCs with varying edge lengths. The scanning electron microscopy (SEM) image of the Ag NCs is shown in Figure S16. In a fixed-size optical cavity, the edge length of Ag NCs directly affects the resonant wavelength of the cavity.[42] As shown in Figure 4a, the SPR peak exhibits a continuous red shift with the increase of the edge length of Ag NCs. Furthermore, the theoretical and experimental SPR peak positions show good agreement (Figure 4b). Figure 4c illustrates the influence of Ag NC edge lengths on the PL spectra of RB (PE-5). The plasmon-induced emission peak (E_m, red peak) was fitted by fixing the peak positions and full width at half-maximum of the two intrinsic fluorescence peaks (580 nm, green peak; 620 nm, orange peak). As the edge length of Ag NCs increased, the plasmon-induced emission peak of RB exhibited a gradual red shift. In Figure S18, we display emission spectra from different particles for each particle size. There are three emission spectra shown for each particle size. The plasmon-induced emission peaks show good consistency for particles with similar sizes. Besides, it is worth noting that, for smaller Ag NC sizes, such as 60 nm, the enhancement is observed in fluorescence. For larger Ag NC sizes, such as 90 nm, the plasmon activates the originally "dark state" phosphorescence (Figure S19). The distinction between phosphorescence and fluorescence can be made by analyzing their respective lifetimes. In addition, we also simulated the radiative behavior of molecules in different resonators (Figure 4d) to jointly reveal the plasmon-molecule interaction mechanism. Both the experimental and simulated results show that the peak positions of the emission spectra can be continuously and strongly modified by controlling the edge length of Ag NCs.

We count the peak λ_{Em} for 54 sets of experimental emission wavelengths (purple spheres) and 6 sets of theoretical emission wavelengths (green squares) as a function of the peak of the SPR spectra (λ_{SPR}) (Figure 4e). The results show that almost all data points appear around the gray dashed line, that is, $\lambda_{Em} = \lambda_{SPR}$, which indicates a linear correlation between the SPR peak position and the induced emission peak position. The induced E_m peak is directly determined by the corresponding single nanoantenna and the peak positions can be regulated over the 200 nm spectrum range.

The energy levels of the molecules remain unchanged. The key to achieving room-temperature phosphorescence lies in enhancing the spontaneous emission rate while maintaining a high quantum yield. The spontaneous emission rate can be significantly enhanced by overlapping the SPR with molecular emission spectra. The key to achieving a high quantum yield is using an appropriately sized nanocavity. The single nanoantenna enhances different parts of the room-temperature emission spectrum of the molecule according to the corresponding SPR spectrum, allowing the molecule to preferentially radiate to specific vibrational energy levels. This ultimately leads to the intelligent tailoring of the molecule's fluorescence−phosphorescence emission properties by plasmon modulation. For the first time, the phosphorescence, which was originally in the "dark state" due to the slow radiation rate and oxygen sensitivity at room temperature, is accelerated in the radiative transition process under the influence of the plasmon, transforming into an ultrafast "bright state".

CONCLUSIONS

This work develops a framework based on optical cavity−molecular interactions for plasmon tailoring the fluorescence−phosphorescence emission. In the presence of SPR, the fluorescence−phosphorescence emission behavior of probe molecules was found to be highly dependent on the size of the metal nanoparticle, the strength of the electromagnetic field at the location of the molecules, and the degree of overlap between the SPR spectrum and the molecular emission spectrum. Both the PL intensity and the fluorescence−phosphorescence emission peak position can be intelligently tailored by precisely constructing the plasmonic nanostructure. Further, we here show experimental and theoretical evidence which supports the exciting prospect of creating materials where the fluorescence and phosphorescence excitation states can be tailored to specific vibrational ground states. Therefore, plasmon-tailored spectroscopic strategies have the potential to expand into more practical application fields.

ASSOCIATED CONTENT

Supporting Information

The Supporting Information is available free of charge at https://pubs.acs.org/doi/10.1021/jacs.3c05496.

Construction of plasmon-tailored spectroscopy; absorption and emission spectra of RB; optimization of Ag NC concentration; mapping of PL spectra; fitting parameters and calculation results; normalized phosphorescence decay time; variation of emission peak area; radiation parameters; and SEM characterization (PDF)

AUTHOR INFORMATION

Corresponding Authors

Jun Yi − *State Key Laboratory of Physical Chemistry of Solid Surfaces, iChEM, College of Chemistry and Chemical Engineering, College of Materials, College of Electronic Science and Engineering, College of Energy, College of Physical Science and Technology, Fujian Key Laboratory of Ultrafast Laser Technology and Applications, Xiamen University, Xiamen 361005, China;* orcid.org/0000-0003-2186-6615; Email: junyi@xmu.edu.cn

Jian-Feng Li − *State Key Laboratory of Physical Chemistry of Solid Surfaces, iChEM, College of Chemistry and Chemical Engineering, College of Materials, College of Electronic Science and Engineering, College of Energy, College of Physical Science and Technology, Fujian Key Laboratory of Ultrafast Laser Technology and Applications, Xiamen University, Xiamen 361005, China; College of Optical and Electronic Technology, China Jiliang University, Hangzhou 310018, China; Innovation Laboratory for Sciences and Technologies of Energy Materials of Fujian Province (IKKEM), Xiamen 361005, China;* orcid.org/0000-0003-1598-6856; Email: Li@xmu.edu.cn

Authors

Wei Peng − *State Key Laboratory of Physical Chemistry of Solid Surfaces, iChEM, College of Chemistry and Chemical Engineering, College of Materials, College of Electronic Science and Engineering, College of Energy, College of Physical Science and Technology, Fujian Key Laboratory of Ultrafast*

Laser Technology and Applications, Xiamen University, Xiamen 361005, China

Yao-Hui Wang − *State Key Laboratory of Physical Chemistry of Solid Surfaces, iChEM, College of Chemistry and Chemical Engineering, College of Materials, College of Electronic Science and Engineering, College of Energy, College of Physical Science and Technology, Fujian Key Laboratory of Ultrafast Laser Technology and Applications, Xiamen University, Xiamen 361005, China*

Jiaxing He − *Department of Chemistry and Key Laboratory for Preparation and Application of Ordered Structural Materials of Guangdong Province, Shantou University, Shantou 515063, China*

Jing-Liang Yang − *College of Physics, Guizhou Province Key Laboratory for Photoelectrics Technology and Application, Guizhou University, Guiyang 550025, China*

Jingyu Wang − *State Key Laboratory of Physical Chemistry of Solid Surfaces, iChEM, College of Chemistry and Chemical Engineering, College of Materials, College of Electronic Science and Engineering, College of Energy, College of Physical Science and Technology, Fujian Key Laboratory of Ultrafast Laser Technology and Applications, Xiamen University, Xiamen 361005, China*

Petar M. Radjenovic − *State Key Laboratory of Physical Chemistry of Solid Surfaces, iChEM, College of Chemistry and Chemical Engineering, College of Materials, College of Electronic Science and Engineering, College of Energy, College of Physical Science and Technology, Fujian Key Laboratory of Ultrafast Laser Technology and Applications, Xiamen University, Xiamen 361005, China*

Jia-Sheng Lin − *State Key Laboratory of Physical Chemistry of Solid Surfaces, iChEM, College of Chemistry and Chemical Engineering, College of Materials, College of Electronic Science and Engineering, College of Energy, College of Physical Science and Technology, Fujian Key Laboratory of Ultrafast Laser Technology and Applications, Xiamen University, Xiamen 361005, China*

Zhilin Yang − *State Key Laboratory of Physical Chemistry of Solid Surfaces, iChEM, College of Chemistry and Chemical Engineering, College of Materials, College of Electronic Science and Engineering, College of Energy, College of Physical Science and Technology, Fujian Key Laboratory of Ultrafast Laser Technology and Applications, Xiamen University, Xiamen 361005, China;* orcid.org/0000-0002-4799-1492

Ming-De Li − *Department of Chemistry and Key Laboratory for Preparation and Application of Ordered Structural Materials of Guangdong Province, Shantou University, Shantou 515063, China;* orcid.org/0000-0002-7568-8300

Fan-Li Zhang − *College of Optical and Electronic Technology, China Jiliang University, Hangzhou 310018, China;* orcid.org/0000-0001-9396-7867

Yue-Jiao Zhang − *State Key Laboratory of Physical Chemistry of Solid Surfaces, iChEM, College of Chemistry and Chemical Engineering, College of Materials, College of Electronic Science and Engineering, College of Energy, College of Physical Science and Technology, Fujian Key Laboratory of Ultrafast Laser Technology and Applications, Xiamen University, Xiamen 361005, China*

Complete contact information is available at: https://pubs.acs.org/10.1021/jacs.3c05496

Notes

The authors declare no competing financial interest.

■ ACKNOWLEDGMENTS

This work was financially supported by the National Natural Science Foundation of China (21925404, T2293692, 22021001, 22104124, 22272140, and 22002128), the Xiamen Science and Technology Plan Project (35022022YJ03), and the Fundamental Research Funds for the Central Universities (20720220117 and 20720220139). We also thank Hao Yin and Hong-Jia Wang for the fruitful discussions.

■ REFERENCES

(1) Huang, L.; Chen, B.; Zhang, X.; Trindle, C. O.; Liao, F.; Wang, Y.; Miao, H.; Luo, Y.; Zhang, G. Proton-Activated "Off-On" Room-Temperature Phosphorescence from Purely Organic Thioethers. *Angew. Chem., Int. Ed.* **2018**, *57*, 16046−16050.

(2) Gao, R.; Mei, X.; Yan, D.; Liang, R.; Wei, M. Nano-photosensitizer based on layered double hydroxide and isophthalic acid for singlet oxygenation and photodynamic therapy. *Nat. Commun.* **2018**, *9*, 2798.

(3) Miao, Q.; Xie, C.; Zhen, X.; Lyu, Y.; Duan, H.; Liu, X.; Jokerst, J. V.; Pu, K. Molecular afterglow imaging with bright, biodegradable polymer nanoparticles. *Nat. Biotechnol.* **2017**, *35*, 1102−1110.

(4) Semeniak, D.; Cruz, D. F.; Chilkoti, A.; Mikkelsen, M. H. Plasmonic Fluorescence Enhancement in Diagnostics for Clinical Tests at Point-of-Care: A Review of Recent Technologies. *Adv. Mater.* **2023**, *35*, 2107986.

(5) Ravetz, B. D.; Pun, A. B.; Churchill, E. M.; Congreve, D. N.; Rovis, T.; Campos, L. M. Photoredox catalysis using infrared light via triplet fusion upconversion. *Nature* **2019**, *565*, 343−346.

(6) Mongin, C.; Garakyaraghi, S.; Razgoniaeva, N.; Zamkov, M.; Castellano, F. N. Direct observation of triplet energy transfer from semiconductor nanocrystals. *Science* **2016**, *351*, 369−372.

(7) Toftegaard, R.; Arnbjerg, J.; Daasbjerg, K.; Ogilby, P. R.; Dmitriev, A.; Sutherland, D. S.; Poulsen, L. Metal-enhanced 1270 nm singlet oxygen phosphorescence. *Angew. Chem., Int. Ed.* **2008**, *47*, 6025−6027.

(8) Bolton, O.; Lee, K.; Kim, H. J.; Lin, K. Y.; Kim, J. Activating efficient phosphorescence from purely organic materials by crystal design. *Nat. Chem.* **2011**, *3*, 415.

(9) Curto, A. G.; Volpe, G.; Taminiau, T. H.; Kreuzer, M. P.; Quidant, R.; van Hulst, N. F. Unidirectional emission of a quantum dot coupled to a nanoantenna. *Science* **2010**, *329*, 930−933.

(10) Gu, L.; Wu, H.; Ma, H.; Ye, W.; Jia, W.; Wang, H.; Chen, H.; Zhang, N.; Wang, D.; Qian, C.; An, Z.; Huang, W.; Zhao, Y. Color-tunable ultralong organic room temperature phosphorescence from a multicomponent copolymer. *Nat. Commun.* **2020**, *11*, 944.

(11) Deng, R.; Qin, F.; Chen, R.; Huang, W.; Hong, M.; Liu, X. Temporal full-colour tuning through non-steady-state upconversion. *Nat. Nanotechnol.* **2015**, *10*, 237−242.

(12) Huang, L.; Liu, L.; Li, X.; Hu, H.; Chen, M.; Yang, Q.; Ma, Z.; Jia, X. Crystal-State Photochromism and Dual-Mode Mechanochromism of an Organic Molecule with Fluorescence, Room-Temperature Phosphorescence, and Delayed Fluorescence. *Angew. Chem., Int. Ed.* **2019**, *58*, 16445−16450.

(13) Wu, H.; Chi, W.; Baryshnikov, G.; Wu, B.; Gong, Y.; Zheng, D.; Li, X.; Zhao, Y.; Liu, X.; Agren, H.; Zhu, L. Crystal Multi-Conformational Control Through Deformable Carbon-Sulfur Bond for Singlet-Triplet Emissive Tuning. *Angew. Chem., Int. Ed.* **2019**, *58*, 4328.

(14) Mishra, H.; Mali, B. L.; Karolin, J.; Dragan, A. I.; Geddes, C. D. Experimental and theoretical study of the distance dependence of metal-enhanced fluorescence, phosphorescence and delayed fluorescence in a single system. *Phys. Chem. Chem. Phys.* **2013**, *15*, 19538−19544.

(15) Zhao, W.; He, Z.; Tang, B. Z. Room-temperature phosphorescence from organic aggregates. *Nat. Rev. Mater.* **2020**, *5*, 869−885.
(16) Ma, X.; Wang, J.; Tian, H. Assembling-Induced Emission: An Efficient Approach for Amorphous Metal-Free Organic Emitting Materials with Room-Temperature Phosphorescence. *Acc. Chem. Res.* **2019**, *52*, 738−748.
(17) Han, S.; Deng, R.; Gu, Q.; Ni, L.; Huynh, U.; Zhang, J.; Yi, Z.; Zhao, B.; Tamura, H.; Pershin, A.; Xu, H.; Huang, Z.; Ahmad, S.; Abdi-Jalebi, M.; Sadhanala, A.; Tang, M. L.; Bakulin, A.; Beljonne, D.; Liu, X.; Rao, A. Lanthanide-doped inorganic nanoparticles turn molecular triplet excitons bright. *Nature* **2020**, *587*, 594−599.
(18) Lin, K. Q.; Yi, J.; Zhong, J. H.; Hu, S.; Liu, B. J.; Liu, J. Y.; Zong, C.; Lei, Z. C.; Wang, X.; Aizpurua, J.; Esteban, R.; Ren, B. Plasmonic photoluminescence for recovering native chemical information from surface-enhanced Raman scattering. *Nat. Commun.* **2017**, *8*, 14891.
(19) Liu, X.; Yi, J.; Yang, S.; Lin, E. C.; Zhang, Y. J.; Zhang, P.; Li, J. F.; Wang, Y.; Lee, Y. H.; Tian, Z. Q.; Zhang, X. Nonlinear valley phonon scattering under the strong coupling regime. *Nat. Mater.* **2021**, *20*, 1210−1215.
(20) Jiang, N.; Zhuo, X.; Wang, J. Active Plasmonics: Principles, Structures, and Applications. *Chem. Rev.* **2018**, *118*, 3054−3099.
(21) Li, C. Y.; Meng, M.; Huang, S. C.; Li, L.; Huang, S. R.; Chen, S.; Meng, L. Y.; Panneerselvam, R.; Zhang, S. J.; Ren, B.; Yang, Z. L.; Li, J. F.; Tian, Z. Q. Smart Ag Nanostructures for Plasmon-Enhanced Spectroscopies. *J. Am. Chem. Soc.* **2015**, *137*, 13784−13787.
(22) Baumberg, J. J.; Aizpurua, J.; Mikkelsen, M. H.; Smith, D. R. Extreme nanophotonics from ultrathin metallic gaps. *Nat. Mater.* **2019**, *18*, 668−678.
(23) Akselrod, G. M.; Argyropoulos, C.; Hoang, T. B.; Ciracì, C.; Fang, C.; Huang, J.; Smith, D. R.; Mikkelsen, M. H. Probing the mechanisms of large Purcell enhancement in plasmonic nanoantennas. *Nat. Photonics* **2014**, *8*, 835−840.
(24) Wang, Y. H.; Zheng, S.; Yang, W. M.; Zhou, R. Y.; He, Q. F.; Radjenovic, P.; Dong, J. C.; Li, S.; Zheng, J.; Yang, Z. L.; Attard, G.; Pan, F.; Tian, Z. Q.; Li, J. F. In situ Raman spectroscopy reveals the structure and dissociation of interfacial water. *Nature* **2021**, *600*, 81−85.
(25) Li, J. F.; Huang, Y. F.; Ding, Y.; Yang, Z. L.; Li, S. B.; Zhou, X. S.; Fan, F. R.; Zhang, W.; Zhou, Z. Y.; Wu, D. Y.; Ren, B.; Wang, Z. L.; Tian, Z. Q. Shell-isolated nanoparticle-enhanced Raman spectroscopy. *Nature* **2010**, *464*, 392−395.
(26) Pallaoro, A.; Braun, G. B.; Moskovits, M. Biotags Based on Surface-Enhanced Raman Can Be as Bright as Fluorescence Tags. *Nano Lett.* **2015**, *15*, 6745−6750.
(27) Siraj, N.; El-Zahab, B.; Hamdan, S.; Karam, T. E.; Haber, L. H.; Li, M.; Fakayode, S. O.; Das, S.; Valle, B.; Strongin, R. M.; Patonay, G.; Sintim, H. O.; Baker, G. A.; Powe, A.; Lowry, M.; Karolin, J. O.; Geddes, C. D.; Warner, I. M. Fluorescence, Phosphorescence, and Chemiluminescence. *Anal. Chem.* **2016**, *88*, 170−202.
(28) Li, J. F.; Li, C. Y.; Aroca, R. F. Plasmon-enhanced fluorescence spectroscopy. *Chem. Soc. Rev.* **2017**, *46*, 3962−3979.
(29) Pelton, M. Modified spontaneous emission in nanophotonic structures. *Nat. Photonics* **2015**, *9*, 427−435.
(30) Hoang, T. B.; Akselrod, G. M.; Argyropoulos, C.; Huang, J.; Smith, D. R.; Mikkelsen, M. H. Ultrafast spontaneous emission source using plasmonic nanoantennas. *Nat. Commun.* **2015**, *6*, 7788.
(31) Rivera, N.; Kaminer, I.; Zhen, B.; Joannopoulos, J. D.; Soljacic, M. Shrinking light to allow forbidden transitions on the atomic scale. *Science* **2016**, *353*, 263−269.
(32) Duan, S.; Rinkevicius, Z.; Tian, G.; Luo, Y. Optomagnetic Effect Induced by Magnetized Nanocavity Plasmon. *J. Am. Chem. Soc.* **2019**, *141*, 13795−13798.
(33) Park, J. E.; Kim, J.; Nam, J. M. Emerging plasmonic nanostructures for controlling and enhancing photoluminescence. *Chem. Sci.* **2017**, *8*, 4696−4704.
(34) Geddes, C. D.; Lakowicz, J. R. Metal-Enhanced Fluorescence. *J. Fluoresc.* **2002**, *12*, 121.
(35) Macia, N.; Bresoli-Obach, R.; Nonell, S.; Heyne, B. Hybrid Silver Nanocubes for Improved Plasmon-Enhanced Singlet Oxygen Production and Inactivation of Bacteria. *J. Am. Chem. Soc.* **2019**, *141*, 684−692.
(36) Hu, S.; Elliott, E.; Sanchez-Iglesias, A.; Huang, J.; Guo, C.; Hou, Y.; Kamp, M.; Goerlitzer, E. S. A.; Bedingfield, K.; de Nijs, B.; Peng, J.; Demetriadou, A.; Liz-Marzan, L. M.; Baumberg, J. J. Full Control of Plasmonic Nanocavities Using Gold Decahedra-on-Mirror Constructs with Monodisperse Facets. *Adv. Sci.* **2023**, *10*, 2207178.
(37) Chen, W.; Zhang, S.; Deng, Q.; Xu, H. Probing of sub-picometer vertical differential resolutions using cavity plasmons. *Nat. Commun.* **2018**, *9*, 801.
(38) Neckers, D. C. Rose Bengal. *J. Photochem. Photobiol., A* **1989**, *47*, 1−29.
(39) Penzkofer, A.; Tyagi, A.; Slyusareva, E.; Sizykh, A. Phosphorescence and delayed fluorescence properties of fluorone dyes in bio-related films. *Chem. Phys.* **2010**, *378*, 58−65.
(40) Li, C. Y.; Duan, S.; Yi, J.; Wang, C.; Radjenovic, P. M.; Tian, Z. Q.; Li, J. F. Real-time detection of single-molecule reaction by plasmon-enhanced spectroscopy. *Sci. Adv.* **2020**, *6*, No. eaba6012.
(41) Ringler, M.; Schwemer, A.; Wunderlich, M.; Nichtl, A.; Kurzinger, K.; Klar, T. A.; Feldmann, J. Shaping emission spectra of fluorescent molecules with single plasmonic nanoresonators. *Phys. Rev. Lett.* **2008**, *100*, 203002.
(42) Readman, C.; de Nijs, B.; Szabo, I.; Demetriadou, A.; Greenhalgh, R.; Durkan, C.; Rosta, E.; Scherman, O. A.; Baumberg, J. J. Anomalously Large Spectral Shifts near the Quantum Tunnelling Limit in Plasmonic Rulers with Subatomic Resolution. *Nano Lett.* **2019**, *19*, 2051−2058.

https://doi.org/10.1021/jacs.3c05496
J. Am. Chem. Soc. 2023, 145, 20381−20388